Supplemental Document

Optics Letters

Single-shot color-multiplexed quantitative phase imaging with Kramers–Kronig relations: supplement

QIAN SHEN,[1,2,3] SHUN ZHOU,[1,2,3] KAIYU DU,[1,2,3] YEFENG SHU,[1,2,3] HABIB ULLAH,[1,2,3] WENZHUO XIE,[1,2,3] TINGXIANG XIONG,[1,2,3] ZHUOSHI LI,[1,2,3] ZANYANG GUAN,[4] YULONG LI,[4] RAN YE,[1,5] YAO FAN,[1,2,3] QIAN CHEN,[3,6] JIASONG SUN,[1,2,3,7] AND CHAO ZUO[1,2,3,*]

[1]*Smart Computational Imaging Laboratory (SCILab), School of Electronic and Optical Engineering, Nanjing University of Science and Technology, Nanjing, Jiangsu Province 210094, China*
[2]*Smart Computational Imaging Research Institute of Nanjing University of Science and Technology, Nanjing, Jiangsu Province 210019, China*
[3]*Jiangsu Key Laboratory of Visual Sensing & Intelligent Perception, Nanjing, Jiangsu Province 210094, China*
[4]*Laser Fusion Research Center, China Academy of Engineering Physics, Mianyang 621900, China*
[5]*School of Computer and Electronic Information, Nanjing Normal University, Nanjing 210023, China*
[6]*State Key Laboratory of Extreme Environment Optoelectronic Dynamic Measurement Technology and Instrument, Taiyuan, Shanxi Province 030051, China*
[7]*sunjiasong@njust.edu.cn*
[*]*zuochao@njust.edu.cn*

Supplement DOI: https://doi.org/10.6084/m9.figshare.32423034

Parent Article DOI: https://doi.org/10.1364/OL.596621

Single-shot color-multiplexed quantitative phase imaging with Kramers-Kronig relations: Supplemental Document

This document provides supplementary information for "Single-shot color-multiplexed quantitative phase imaging with Kramers-Kronig relations".

A. Color-multiplexed illumination strategy in CMKK-QPI

The spectrum patterns shown in Fig. 1(c) illustrate the Fourier-domain sampling mechanism of CMKK-QPI under color-multiplexed oblique illumination. As shown in Fig. S1, different oblique illumination angles correspond to distinct incident wavevectors and therefore shift the object spectrum to different locations in Fourier space. The sampled sub-spectra are determined by the illumination angle, wavelength, and objective numerical aperture.

Under color-multiplexed illumination, these angularly diverse measurements are encoded into a single color exposure while remaining separable through the R/G/B channels of the sensor [1, 2]. Therefore, the spectrum patterns indicate which spatial-frequency regions are captured under each illumination condition and how these shifted sub-spectra jointly contribute to the synthetic-aperture reconstruction.

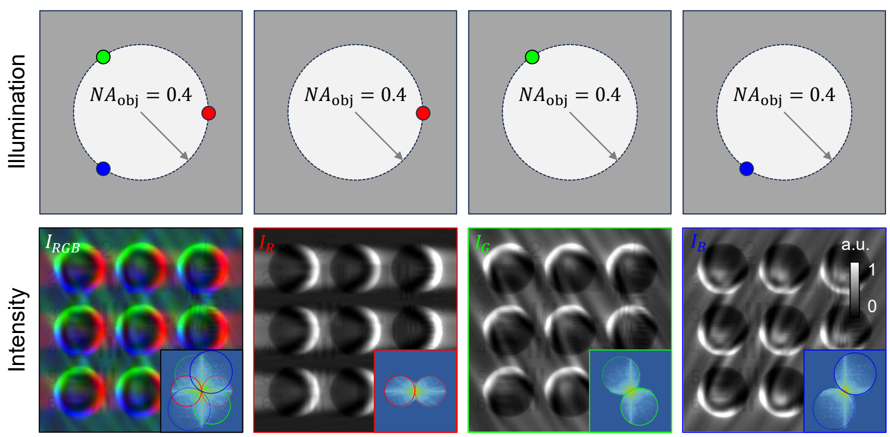

Fig. S1. Fourier-domain sampling mechanism in CMKK-QPI. Different oblique illumination angles produce distinct shifts of the object spectrum in Fourier space. The corresponding illumination configurations, intensity distributions, and Fourier spectra show how angularly diverse spatial-frequency information is encoded into a single color exposure.

B. Phase unwrapping and wavelength normalization for CMKK-QPI

For large-phase objects, the phase may exceed 2π, making phase unwrapping necessary for accurate quantitative phase retrieval. In addition, in color-multiplexed imaging, the recovered phase from different wavelengths must be normalized to a common reference wavelength before combination. Assuming negligible chromatic dispersion within the visible range, the normalized phase at wavelength λ_c can be written as

$$\phi_{c,G}(\mathbf{r}) = \frac{\lambda_c}{\lambda_G}\,\tilde{\phi}_c(\mathbf{r}), \qquad c \in \{R, G, B\}, \tag{S1}$$

where $\tilde{\phi}_c(\mathbf{r})$ denotes the unwrapped phase of spectral component c, and $\phi_{c,G}(\mathbf{r})$ denotes the phase normalized to the reference wavelength λ_G.

Following the iterative reconstruction strategy of the iKK-QPI framework [3], the CMKK-QPI procedure with phase unwrapping and wavelength normalization is summarized in Algorithm S1. The operators used in Algorithm S1 are defined as follows: $\mathcal{KK}$ denotes the Kramers-Kronig (KK) [4–11] reconstruction operator, $\arg(\cdot)$ denotes phase extraction, $\text{unwrap}(\cdot)$ denotes the phase-unwrapping operator [12], $\mathcal{SA}$ denotes the synthetic-aperture composition operator and $\mathcal{SA}_c^{-1}$ denotes the low-pass filtering operation for selecting the sub-spectrum of spectral component c corresponding to its illumination angle. In addition, $\phi_c(\mathbf{r})$ denotes the wrapped phase, $\tilde{\phi}_c(\mathbf{r})$ denotes the unwrapped phase, $U_c(\mathbf{r})$ denotes the complex field of spectral component c, $\tilde{U}_{c,G}(\mathbf{r})$ denotes the corresponding complex field after phase unwrapping and wavelength normalization, and $O_{\text{rec}}(\mathbf{r})$ denotes the reconstructed full-field complex amplitude. The superscripts 0, n, and $n+1$ denote the initialization, the current iteration, and the updated iteration, respectively.

Algorithm S1. CMKK-QPI reconstruction with phase unwrapping and wavelength normalization

Require: intensity distributions $I_c(\mathbf{r})$, wavelengths λ_c for $c \in \{R, G, B\}$, reference wavelength λ_G

$$U_c^0(\mathbf{r}) = \mathcal{KK}[I_c(\mathbf{r})], \qquad c \in \{R, G, B\}$$

$$\phi_c^0(\mathbf{r}) = \arg\big(U_c^0(\mathbf{r})\big), \qquad c \in \{R, G, B\}$$

$$\tilde{\phi}_c^0(\mathbf{r}) = \text{unwrap}\big(\phi_c^0(\mathbf{r})\big), \qquad c \in \{R, G, B\}$$

$$\phi_{c,G}^0(\mathbf{r}) = \frac{\lambda_c}{\lambda_G}\, \tilde{\phi}_c^0(\mathbf{r}), \qquad c \in \{R, G, B\}$$

$$\tilde{U}_{c,G}^0(\mathbf{r}) = \left|U_c^0(\mathbf{r})\right| \exp\left[i\, \phi_{c,G}^0(\mathbf{r})\right], \qquad c \in \{R, G, B\}$$

$$O_{\text{rec}}^0(\mathbf{r}) = \mathcal{SA}\left[\tilde{U}_{R,G}^0(\mathbf{r}), \tilde{U}_{G,G}^0(\mathbf{r}), \tilde{U}_{B,G}^0(\mathbf{r})\right]$$

for $n = 0, 1, 2, \ldots$ until convergence **do**

$$U_c^n(\mathbf{r}) = \mathcal{SA}_c^{-1}[O_{\text{rec}}^n(\mathbf{r})], \qquad c \in \{R, G, B\}$$

$$U_c^{n+1}(\mathbf{r}) = \exp\left(\frac{1}{2}\log I_c(\mathbf{r}) + i\,\text{Im}[\log U_c^n(\mathbf{r})]\right), \qquad c \in \{R, G, B\}$$

$$\phi_c^{n+1}(\mathbf{r}) = \arg\big(U_c^{n+1}(\mathbf{r})\big), \qquad c \in \{R, G, B\}$$

$$\tilde{\phi}_c^{n+1}(\mathbf{r}) = \text{unwrap}\big(\phi_c^{n+1}(\mathbf{r})\big), \qquad c \in \{R, G, B\}$$

$$\phi_{c,G}^{n+1}(\mathbf{r}) = \frac{\lambda_c}{\lambda_G}\, \tilde{\phi}_c^{n+1}(\mathbf{r}), \qquad c \in \{R, G, B\}$$

$$\tilde{U}_{c,G}^{n+1}(\mathbf{r}) = \left|U_c^{n+1}(\mathbf{r})\right| \exp\left[i\, \phi_{c,G}^{n+1}(\mathbf{r})\right], \qquad c \in \{R, G, B\}$$

$$O_{\text{rec}}^{n+1}(\mathbf{r}) = \mathcal{SA}\left[\tilde{U}_{R,G}^{n+1}(\mathbf{r}), \tilde{U}_{G,G}^{n+1}(\mathbf{r}), \tilde{U}_{B,G}^{n+1}(\mathbf{r})\right]$$

return $O_{\text{rec}}(\mathbf{r})$

C. Simulation validation of CMKK-QPI on a large-phase object

To further validate the reconstruction performance of CMKK-QPI, we performed a simulation using a weakly absorbing complex sample with a maximum phase delay of 5 rad, as shown in Supplementary Fig. S2(a). The same color-multiplexed oblique illumination scheme as that used in the experiment was adopted to generate the corresponding measurements.

The reconstruction obtained by the KK relations-based method is shown in Fig. S2(b). The KK relations-based method fails to recover the true morphology of the object and exhibits pronounced errors in the phase-wrapping regions. These phase errors also lead to evident distortions in the reconstructed amplitude at the corresponding locations, indicating that the reconstruction of both amplitude and phase is degraded when the wrapped phase is not properly handled. By contrast, the CMKK-QPI result in Fig. S2(c) shows much better agreement with the ground truth after iterative refinement. As further shown by the phase error curve in Supplementary Fig. S2(d), the reconstruction error decreases rapidly during the first few iterations and then gradually converges. This behavior is consistent with the experimental observation that only a small number of iterations is sufficient for stable reconstruction. These simulation results further verify the effectiveness of CMKK-QPI for accurate quantitative phase reconstruction of complex samples.

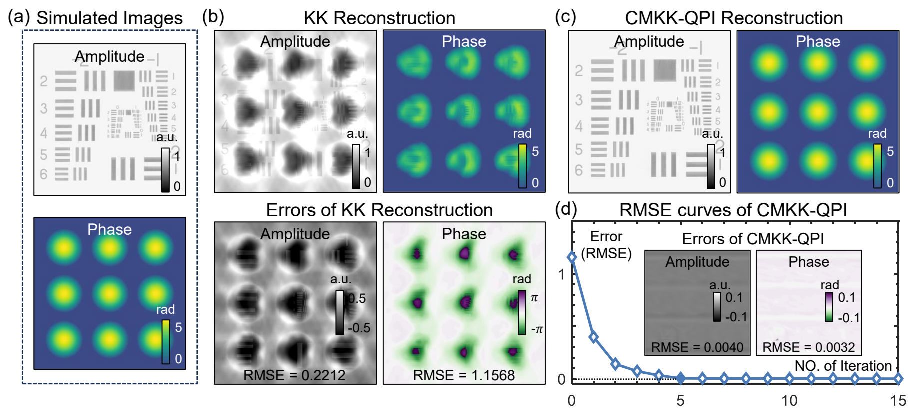

Fig. S2. Simulation validation of CMKK-QPI. (a) Simulated images. (b) Amplitude and phase reconstructed by the KK relations-based method, together with the corresponding error map. (c) Amplitude and phase reconstructed by CMKK-QPI. (d) Phase RMSE curve versus the iteration number.

D. Effect of alternating illumination in dynamic live-cell imaging

To further clarify the role of the alternating illumination strategy in dynamic live-cell imaging, we compared the reconstruction results of live HeLa cells obtained from a single frame under one illumination pattern and from two adjacent frames acquired under alternating illumination patterns. As shown in Fig. S3, the single-frame reconstruction already provides good image quality and clearly resolves the overall cellular morphology as well as major intracellular features, confirming that CMKK-QPI remains effective under the single-shot acquisition scheme. When the information from two adjacent frames is combined using the sliding-window strategy, the reconstructed image shows a modest further improvement in quality. In particular, the cell boundary and intracellular structures appear slightly clearer, and the reconstruction becomes more uniform and stable. Importantly, this improvement is achieved without sacrificing the imaging speed, since no additional exposures are introduced per frame. These results indicate that the alternating illumination strategy is not required for basic single-shot CMKK-QPI reconstruction, but serves as an optional enhancement for dynamic live-cell imaging by improving Fourier-space coverage across adjacent frames while preserving the acquisition frame rate.

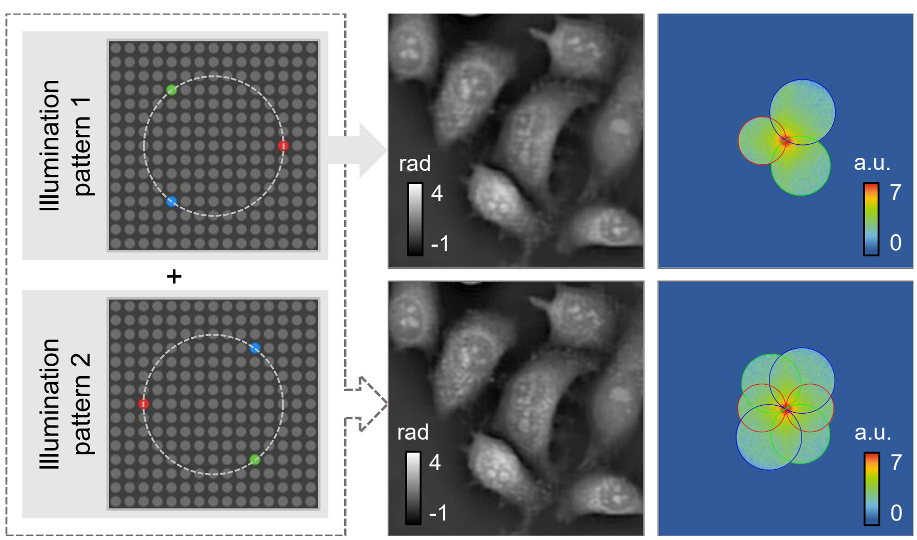

Fig. S3. Comparison of single-frame reconstruction and sliding-window reconstruction with alternating illumination in dynamic live-cell imaging of HeLa cells.

REFERENCES

1. J. Sun, Q. Chen, J. Zhang, *et al.*, "Single-shot quantitative phase microscopy based on color-multiplexed fourier ptychography," Opt. Lett. **43**, 3365–3368 (2018).
2. W. Lee, D. Jung, S. Ryu, and C. Joo, "Single-exposure quantitative phase imaging in color-coded led microscopy," Opt. Express **25**, 8398–8411 (2017).
3. Q. Shen, J. Sun, S. Zhou, *et al.*, "Iterative kramers-kronig method for non-interferometric quantitative phase imaging: beyond the first-order born and rytov approximations," Opt. Lett. **50**, 1144–1147 (2025).
4. Y. Baek and Y. Park, "Intensity-based holographic imaging via space-domain kramers-kronig relations," Nat. Photonics **15**, 354–360 (2021).
5. C. Shen, M. Liang, A. Pan, and C. Yang, "Non-iterative complex wave-field reconstruction based on kramers-kronig relations," Photonics Res. **9**, 1003–1012 (2021).
6. Z. Huang and L. Cao, "High bandwidth-utilization digital holographic multiplexing: an approach using kramers-kronig relations," Adv. Photonics Res. **3**, 2100273 (2022).
7. Y. Li, X. Wen, M. Sun, *et al.*, "Spectrum sampling optimization for quantitative phase imaging based on kramers-kronig relations," Opt. Lett. **47**, 2786–2789 (2022).
8. C. Lee, Y. Baek, H. Hugonnet, and Y. Park, "Single-shot wide-field topography measurement using spectrally multiplexed reflection intensity holography via space-domain kramers-kronig relations," Opt. Lett. **47**, 1025–1028 (2022).
9. X. Chen, S. Yao, X. Yan, *et al.*, "Single-shot resolution-enhancement quantitative phase imaging based on kramers-kronig relations," Opt. Lett. **48**, 3563–3566 (2023).
10. X. Chen, S. Yao, J. Song, *et al.*, "Full-angle single-shot quantitative phase imaging based on kramers-kronig relations," Opt. Lett. **49**, 3512–3515 (2024).
11. Y. Wang, Y. Li, Z. Li, *et al.*, "Structured illumination microscopy based on kramers-kronig relations for quantitative phase reconstruction," Opt. Lett. **49**, 6801–6804 (2024).
12. M. A. Herraez, D. R. Burton, M. J. Lalor, and M. A. Gdeisat, "Fast two-dimensional phase-unwrapping algorithm based on sorting by reliability following a noncontinuous path," Appl. Opt. **41**, 7437–7444 (2002).